E-field extraction from H- and H- near field values by using plane wave spectrum method

B. Ravelo, Z. Riah, D. Baudry, B. Mazari

E-field extraction from Hx- and Hy- near field values by using plane wave spectrum method

B. Ravelo*, Z. Riah, D. Baudry and B. Mazari

IRSEEM - EA 4353, Engineering School ESIGELEC,
Technopole de Madrillet, Avenue Galilée, BP 10024,
76801 Saint-Etienne-du-Rouvray Cedex, France,
Tel: +33.(0)2.32.91.59.71,
Fax: +33.(0)2.32.91.58.59.

*blaise.ravelo@esigelec.fr (the corresponding author)
zoheir.riah@esigelec.fr
david.baudry@esigelec.fr
belahcene.mazari@esigelec.fr

Abstract- This paper deals with a technique for calculating the 3D E-field components knowing only the two components (H_x and H_y) of the H-field in near-zone. The originality of the under study technique lies on the possibility to take into account the evanescent wave influences. The presented E-field extraction process is based on the exploitation of the Maxwell-Ampere relation combined with the plane wave spectrum (PWS) method. The efficiency of the proposed technique is evidenced by comparing the E-field deduced from H-field and the own E-field radiated by the association of electrical- and also magnetic- elementary dipoles in different configurations by using Matlab text programming environment. In addition, as a concrete demonstrator, the concept was also validated with the computation of EM-wave radiated by an open-end microstrip transmission line. As result of comparison, very good agreement between the exact E-field and that one extracted from the H-field was realized by considering the near-field scanned at the height, z = 5 mm and 8 mm above the under test structure at the operating frequency, f = 1 GHz. The presented technique can simplify the difficulties about the E-near-field measurement in EMC applications.

Keywords- E-field extraction, EMC application, Evanescent wave, Maxwell-Ampere relation, Near-field, Plane wave spectrum.

1. INTRODUCTION

The ability to achieve accurate results of electromagnetic (EM) field measurement becomes an important stage for dealing with the EM compatibility (EMC) issues of numerous electronic equipments, including power- and digital-systems. The EMC investigation permits the prevention of the misbehavior of electronic circuits to cope with the inadvertent EM radiation [1-3]. In this scope, international standards have been established in order to ensure the performance, reliability and the electrical safety of certain embedded electronic systems, for example, to avoid the influence of the radio wave interference [4-6]. To study and estimate this EM interference (EMI), numerous studies have been conducted on this topic, in particular, for the modeling and the treatment of the magnetic or H-field radiated both in near- and far-field domains [7-14]. Nonetheless in practice, the magnetic field measurement is generally easier and more precise to carry out because of the facility of the loop probe design and modeling. Till now, due to the coupling and sensitivity problems of the electric dipole probes, few papers were published in the literature for the measurement techniques of the electric or E- near-field at the RF frequencies. In fact, this type of EM field appears when the distance between the source and the targeted point, R is widely less than the wavelength, λ ($R < \lambda/10$). The particularity of this near-field case is that the evanescent wave should be taken into account. The measurement of this EM wave is generally critical for the field scan with submillimeter resolutions. In practice, that case should be achieved for the test of miniaturized electronic device in radiating emission. Currently, the measurement process of this type of E- near-field emission remains a challenge between research engineers.

As a solution of this technical roadblock, an easy computation technique allowing the extraction of the E-field components, E_x, E_y and E_z of course in 3D-space, from only the horizontal components, H_x and H_y of the H-field in near-zone is introduced in this article. The proposed calculation methodology is fundamentally based on the use of the well-known plane wave spectrum (PWS) principle [15-20] applied to the classical Maxwell-Ampere relation. As reported in [16], the theory and the application mostly in far-field domain of this PWS method have been analytically introduced and developed since the early 1970s. By using the PWS transform which is similar to the fast Fourier transform, it is possible to decompose any 2D mapping of EM wave as being the sum of plane waves propagating in different directions [15-25]. Consequently, all useful theorems specific to the physical plane waves can be applied to the PWS components of any type of propagative or evanescent physical waves and then, through inverse PWS (IPWS) calculation, one can turn back to the real space field mapping. As example, recently, an experimental validation of a simple application of PWS method for the determination of the magnetic field at the different heights, $z > 0$ (far-field) above the tested and radiating devices from the simulated or measured near-field data at the height, $z = 0$ has been performed [23-25]. Moreover, as described in [15], another application concerning Maxwell-Ampere relation was also invoked. But in this document, it was basically employed for the far-field approach. But, we recall that the simplicity of this kind of test and analytical study is that the evanescent waves can be neglected. In our knowledge, so far, no study and no concrete result have never been published in the literature for the extraction of the E-field from H-field in near-field domain.

For this reason, the present paper is introduced. It is aimed at the development of the technique for extracting the 3D E-field components calculation from 2D H-field components. For the better understanding, this paper is structured as follows; Section 2 is consecrated to the methodological analysis of the proposed technique. In order to verify the efficiency of the method, we use basic test configurations composed of elementary electric and magnetic dipoles. This allows to compare easily the analytical results of the E- and H-fields and the under treated

approach. The E-field components obtained from H_x and H_y components are presented and commented in section 3. As a concrete application, the proposed technique is also validated in section 4 by considering the EM field radiated by an open-end transmission line (TL) implemented in microstrip planar technology. Lastly, section 5 is the conclusion of this work.

2. DESCRIPTION OF THE PROPOSED EM-FIELD CALCULATION TECHNIQUE

To get a better readability, this section is divided in three different subsections. First, subsection 2.1 depicts the theoretical concepts highlighting how to exploit the plane wave spectrum (PWS) theory combined with Maxwell-Ampere relation for the computation of E-field from the H-field. Then, subsection 2.2 focus is on the determination of the wave vector adequate to the geometrical parameters deemed during the mapping of the given H-field components, H_x and H_y. Then, last subsection details succinctly the description of here presented E-field computation technique methodology.

2.1. Background on the PWS theory and the Maxwell-Ampere relation

It is well-known that according to Maxwell-Ampere law, in any EM medium characterized by an absolute permittivity, ε and permeability, μ_0 and without current source, the E- and H-field vectors should satisfy the following equation:

$$\overrightarrow{rot}\,\vec{H} = \varepsilon \frac{\partial \vec{E}}{\partial t}. \tag{1}$$

For starting, let us assume the wave vector, $\vec{k}$ referenced in the classical rectangular coordinate system ($Oxyz$) with the unit vectors, $\overrightarrow{u_x}$, $\overrightarrow{u_y}$ and $\overrightarrow{u_z}$:

$$\vec{k} = k_x \overrightarrow{u_x} + k_y \overrightarrow{u_y} + k_z \overrightarrow{u_z}. \tag{2}$$

So, the modulus of this wave vector or the wave number is given by:

$$k = \sqrt{k_x^2 + k_y^2 + k_z^2} = \frac{2\pi}{\lambda}, \tag{3}$$

with $\lambda = v/f$, is the wavelength at the operating frequency, f, in the EM-medium characterized by the wave speed, v. Thanks to the PWS theory, as reported in [15-20], these EM fields can be written as being the sum of its PWS components here denoted, $\overrightarrow{F_e}(k_x,k_y)e^{-jk_z z}$ and $\overrightarrow{F_h}(k_x,k_y)e^{-jk_z z}$ with j is as imaginary number, $\sqrt{-1}$. So that, in 2D mapping plan, the E- and H-field are mathematically defined as:

$$\vec{E}(x,y,z)=\frac{1}{4\pi^2}\int_{-\infty}^{\infty}\int_{-\infty}^{\infty}[\overrightarrow{F_e}(k_x,k_y)e^{-jk_z z}]e^{-j(k_x x+k_y y)}dk_x dk_y\,, \tag{4-a}$$

$$\vec{H}(x,y,z)=\frac{1}{4\pi^2}\int_{-\infty}^{\infty}\int_{-\infty}^{\infty}[\overrightarrow{F_h}(k_x,k_y)e^{-jk_z z}]e^{-j(k_x x+k_y y)}dk_x dk_y\,. \tag{4-b}$$

At noted that inversely, the inverse PWS (IPWS) of E- and H-field are, respectively, written as:

$$\overrightarrow{F_e}(k_x,k_y)=\int_{-\infty}^{\infty}\int_{-\infty}^{\infty}[\vec{E}(x,y,z)]\,e^{j(k_x x+k_y y)}dxdy\,, \tag{5-a}$$

$$\overrightarrow{F_h}(k_x,k_y)=\int_{-\infty}^{\infty}\int_{-\infty}^{\infty}[\vec{H}(x,y,z)]\,e^{j(k_x x+k_y y)}dxdy\,. \tag{5-b}$$

As argued earlier to calculate the E-field, one should exploit the Maxwell-Ampere relation expressed in (1). Subsequently, substituting (4-a) and (4-b) into (1) yields the vectorial integro-differential equation as delineted below:

$$\overrightarrow{rot}\left\{\int_{-\infty}^{\infty}\int_{-\infty}^{\infty}[\overrightarrow{F_h}(k_x,k_y)e^{-jk_z z}]e^{-j(k_x x+k_y y)}dk_x dk_y\right\}=\varepsilon\frac{\partial}{\partial t}\left\{\int_{-\infty}^{\infty}\int_{-\infty}^{\infty}[\overrightarrow{F_e}(k_x,k_y)e^{-jk_z z}]e^{-j(k_x x+k_y y)}dk_x dk_y\right\}. \tag{6}$$

Because of linearity and also the natures of $\overrightarrow{F_h}(k_x,k_y)$ and $\overrightarrow{F_e}(k_x,k_y)$ waves, this equation implies also the mathematical relation:

$$\overrightarrow{rot}[\overrightarrow{F_h}(k_x,k_y)]=\varepsilon\frac{\partial[\overrightarrow{F_e}(k_x,k_y)]}{\partial t}\,. \tag{7}$$

According to the physical theory of plane wave propagation, one recalls that when $\overrightarrow{F_h}$ and $\overrightarrow{F_e}$ are monochromatic waves, the previous space-time operators will be transformed as follows:

$$\overrightarrow{rot}(\overrightarrow{F_h})=-j\vec{k}\wedge\overrightarrow{F_h}\,, \tag{8}$$

$$\frac{\partial\overrightarrow{F_e}}{\partial t}=j\omega\overrightarrow{F_e}\,. \tag{9}$$

The fusion of these three last expressions yields the here below formula enabling as well, the extraction of the E-field components, E_x, E_y and E_z from H_x, H_y and H_z:

$$\overrightarrow{F_e}(k_x,k_y)=\frac{-\vec{k}\wedge\overrightarrow{F_h}(k_x,k_y)}{\omega\varepsilon}\Rightarrow\begin{cases}F_{ex}=\dfrac{k_zF_{hy}-k_yF_{hz}}{\omega\varepsilon}\\ F_{ey}=\dfrac{k_xF_{hz}-k_zF_{hx}}{\omega\varepsilon}\\ F_{ez}=\dfrac{k_yF_{hx}-k_xF_{hy}}{\omega\varepsilon}\end{cases}. \tag{10}$$

Hence, from the calculated $\overrightarrow{F_e}$, one can infer the corresponding space E-field vector toward above expression (4-a). Otherwise, as argued previously, it is well-known that if $\overrightarrow{F_h}$ behaves as a plane wave, the vectors, $\vec{k}$ and $\overrightarrow{F_h}$ must be perpendicular or mathematically speaking, $\vec{k}.\overrightarrow{F_h}=0$. It means that by developing this scalar product, one can determine the *z*-components of $\overrightarrow{F_h}$ from the following relation:

$$k_xF_{hx}+k_yF_{hy}+k_zF_{hz}=0\quad\Rightarrow\quad F_{hz}=-\frac{k_xF_{hx}+k_yF_{hy}}{k_z}. \tag{11}$$

From where, one can evaluate the third component, H_z, of the vector, $\overrightarrow{H}$ from H_x and H_y, by using the PWS-definition expressed in (4-b). It raises then:

$$H_z(x,y,z)=\frac{-1}{4\pi^2}\int_{-\infty}^{\infty}\int_{-\infty}^{\infty}\frac{k_xF_{hx}+k_yF_{hy}}{k_z}e^{-j(k_xx+k_yy+k_zz)}dk_xdk_y. \tag{12}$$

During the programming of this double integral in discrete way, an accurate attribution of the wave vector components is fundamentally important. To achieve a good insight on this wave vector computation, the strategy of k_x-, k_y- and k_z-deductions from the considered mapping H-field geometrical parameters is devoted in the next subsection.

2.2. Determination of the wave vector according to the considered discrete geometrical parameters

In the remainder of this paper, as explained in Fig. 1, one assumes as $L_x = x_{max}$ and $L_y = y_{max}$, the dimensions of the considered mapping plan where H_x and H_y maps are supposed predefined. In practice, obviously, the continuous geometrical parameters, *x* and *y* belong respectively, in the intervals, $[0,x_{max}]$ and $[0,y_{max}]$.

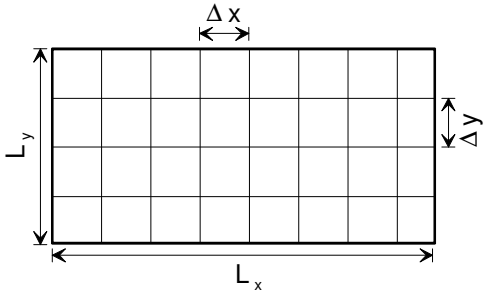

Fig. 1: Representation of the considered mapping plan (parallel to X-Y plane) geometrical parameters.

Thus, as presented in [24-25], we point out that during the implementation of the numerical computation of the previous relations into Matlab text programming environment, x and y should be replaced by their discrete values $n_x\Delta x$ and $n_y\Delta y$, respectively. Δx and Δy denote respectively, the space grid resolutions of x and y. Furthermore, n_x and n_y are integer numbers varying respectively, from 1 to $n_{x\max} = \text{int}(x_{max}/\Delta x)$ and to $n_{y\max} = \text{int}(y_{max}/\Delta y)$, with int($x$) is the lowest integer greater than the real, x. In that case, the discretized horizontal wave vector components will be expressed as follows:

$$k_x = \frac{2\pi}{n_x \Delta x}, \tag{13}$$

$$k_y = \frac{2\pi}{n_y \Delta y}. \tag{14}$$

Substantially, in the considered mapping field plan with (L_x x L_y)-dimensions, these two wave vector components can vary from $(k_{x\min} = -\pi/\Delta x, k_{y\min} = -\pi/\Delta y)$ to $(k_{x\max} = \pi/\Delta x, k_{y\max} = \pi/\Delta y)$ step $(\Delta k_x = 2\pi/L_x, \Delta k_y = 2\pi/L_y)$. Otherwise, the last wave vector component, k_z is merely determined from (3):

$$k_z = \begin{cases} \sqrt{k^2 - k_x^2 - k_y^2} \; if \; k_x^2 + k_y^2 < k^2 \\ -j\sqrt{k_x^2 + k_y^2 - k^2} \; if \; k_x^2 + k_y^2 > k^2 \end{cases}. \tag{15}$$

One can perceive that when $k_x^2 + k_y^2 < k^2$, k_z is a real positive. Therefore, it is clear that the quantity, $e^{-jk_z z}$ corresponds to the behavior of propagative wave. In the contrary case, $k_x^2 + k_y^2 > k^2$, the term, $\sqrt{k_x^2 + k_y^2 - k^2}$ is a real positive, mathematically, it implies that $-j\sqrt{k_x^2 + k_y^2 - k^2}$ is a purely imaginary quantity. This minus sign was intentionally assigned for the achievement of the real case, the decrease of the EM-field value when moving away from the radiating source (z-increasing). So, the quantity, $e^{-jk_z z}$ should correspond to a real term decreasing with z. In that case, the associated EM-waves will be evanescent. Meanwhile, if the step values, Δk_x and Δk_y are greater than the wave number, k, the EM-field PWS data must be completely evanescent. It is interesting to point out that the contribution of the evanescent waves cannot be neglected when working in near-field. We have this type of radiated field if the distance between the radiating source and the point where the EM-field radiation is calculated is lower than λ/10. To avoid this unexpected case, one must choose the geometrical parameters, L_x and L_y, and the space resolutions, Δx and Δy enabling to reach the following requirement:

$$\max(\Delta k_x, \Delta k_y) < k = \frac{2\pi}{\lambda}. \tag{16}$$

Knowing the wave vector component, k_z, which includes the propagative- and evanescent-wave fields as defined in (15), one can calculate first, the H_z-PWS via expression (11) and even the own value of H_z by using

expression (12). Second, one can determine directly the PWS of the E-field via expression (10) and involving then, the expected space E-field with formula (4-a).

2.3. Methodology of the proposed computation technique

The methodology of the investigated E-field computation technique is summarized by the flow chart stated in Fig. 2. One can see clearly that it is executed successively in four different steps:

- **i.** Step 1 is the attribution of the H-near-field components, H_x and H_y as input-data, in parallel with the numerical computation of the wave vector components, k_x, k_y and k_z, of course, knowing the geometrical parameters of the mapping plan located in certain distance, z_0 of the radiating DUT.
- **ii.** Step 2 is simply the calculation of H-field PWS defined previously in (5-b).
- **iii.** Step 3 is the application of Maxwell-Ampere relation expressed in (10) prior to the determination of E-field PWS components, F_{ex}, F_{ey} and F_{ez}.
- **iv.** Step 4 is the computation of the own E-field value through the PWS-operation introduced in (4-a).

It is noteworthy that during the use of the presented calculation technique, the given H-field components, $H_{x,y,z}$ and their PWS, $F_{hx,y,z}$ must trend to zero, respectively, at the extremal values, $x_{min,max}$ and $y_{min,max}$, and $k_{xmin,max}$ and $k_{ymin,max}$, in order to minimize the edge effects. Contrarily to the computation techniques in far-field ($z_0 > \lambda/10$), here, the negligence of the evanescent waves during the computation of the PWS transform of the E- or H-fields can falsify the results of the computed E-field, of course, in the case of near-field radiation.

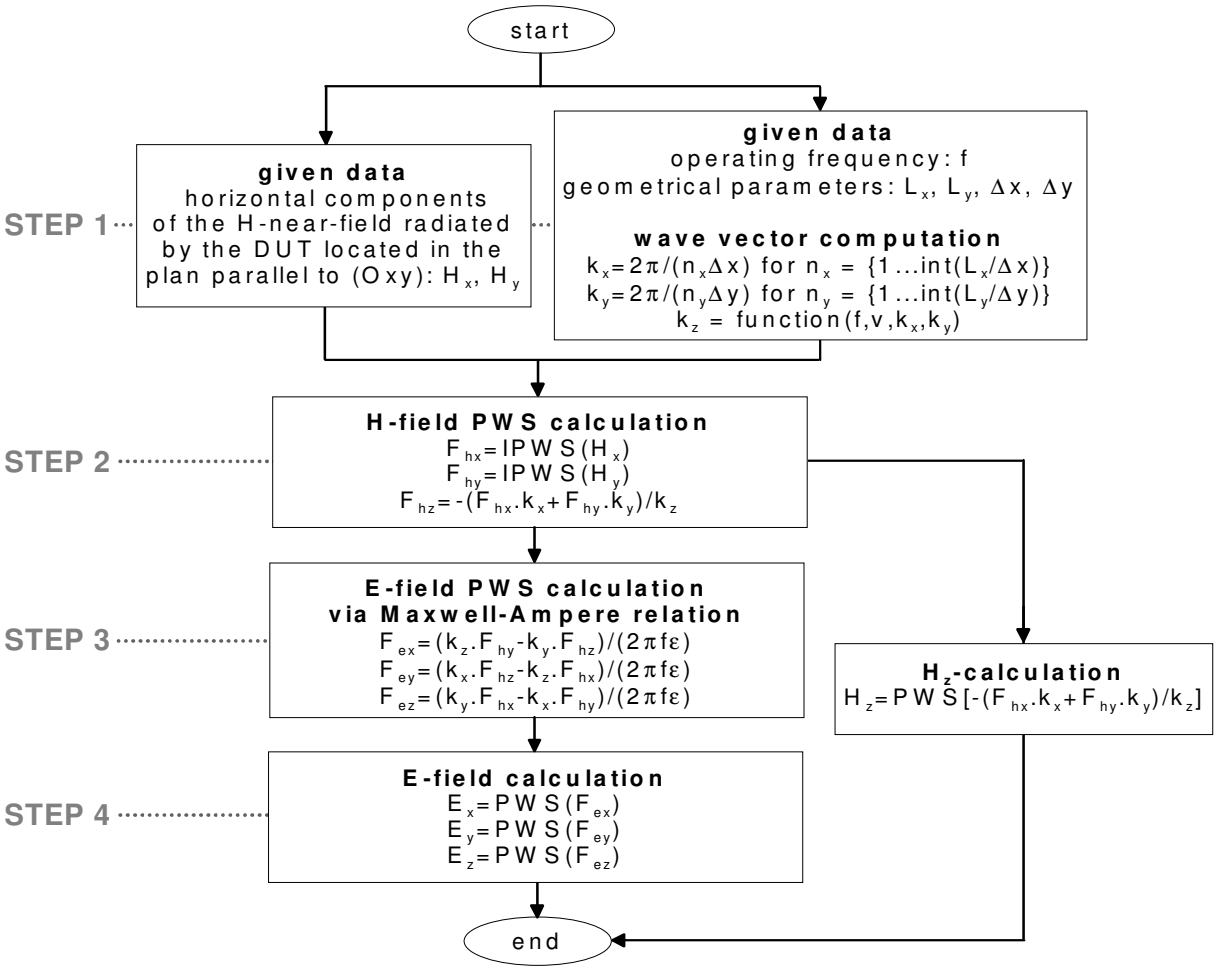

Fig. 2: Flow chart summarizing the proposed methodology of the E-field extraction.

In order to demonstrate the relevance of all this theoretical prediction concept, comparative results between the exact E-field components and those obtained from the PWS calculation are laid out and discussed in the two next sections by considering first, the association of elementary electric and magnetic dipoles, and second, an open-end TL.

3. APPLICATION WITH ELEMENTARY ELECTRIC- AND MAGNETIC- DIPOLES

Figs 3.a and 3.b below depict the configuration of the under study configuration of the electric and magnetic dipoles respectively, and flowed by current with magnitude, I = 1A and frequency, f = 1 GHz. It is worth noting that different arbitrary associations of EM dipoles were chosen for creating more realistic behaviors of near-field cartographies similar to those radiated by the concrete electronic boards. As illustrated in Fig. 3.a, the magnetic dipole loops are aligned along the x-axis and placed at the d-distant points, $M_{1,2,3}$. To generate more general field map behavior, the directions of each dipole were set differently (in x-, z- and y-directions for M_1, M_2 and M_3 respectively). As described in top view of Fig. 3.b, the electric wire dipoles are positioned tangentially to the R = 5 mm radius circle at the points $E_1(R, 0, 0)$, $E_2(R.cos(2\pi/3), R.sin(2\pi/3), 0)$ and $E_3(R.cos(4\pi/3), R.sin(4\pi/3), 0)$ in (Oxy) horizontal plane.

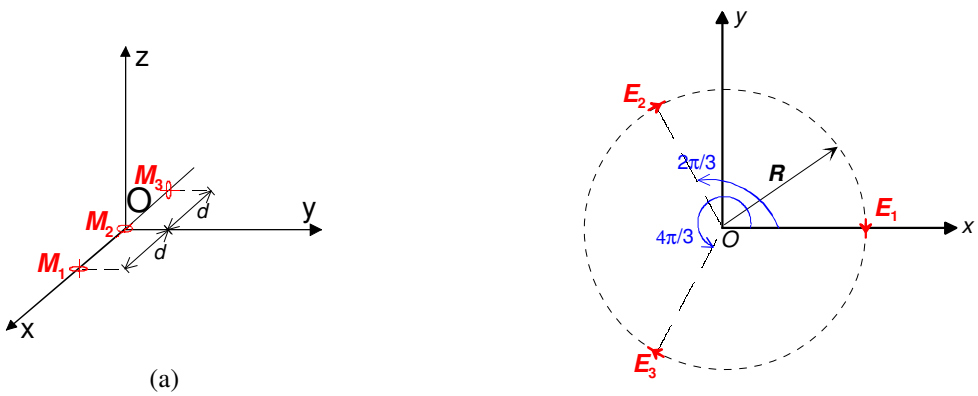

Fig. 3: Configurations of the considered association: (a) magnetic dipole loops (a = 0.2 mm, d = 10 mm) and (b) top view of electric dipole wires (l = 0.5 mm, R = 5 mm).

After running the Matlab program emulated from the text editor of the analytical formulas governing EM field radiation established in [15], one gets the H-field maps of Fig. 4.a. This figure shows the cartography of the H-field radiated by the dipoles of Fig. 3.a in the horizontal plan with dimensions, L_x x L_y = 65 mm x 65 mm placed at the height, z = 8 mm above the dipoles. By implementing and executing the Matlab programming the different steps indicated in flow chart introduced in Fig. 2, we have the second line of the E_x, E_y and E_z component maps of Fig. 4.b. One can find that the calculated E-field components are well-correlated to the direct E-field from the formulas defined in [15]. In order to highlight the relevance of the obtained results, profiles of these three E-field components are also plotted in Fig. 4.c in the vertical cut plane placed, x = 6 mm.

By considering the other configuration of the electric dipole wires shown in Fig. 3.b, one generates the field maps computed in the horizontal plan with dimensions, L_x x L_y = 60 mm x 80 mm, placed at the height, z = 8 mm displayed in Figs. 5.

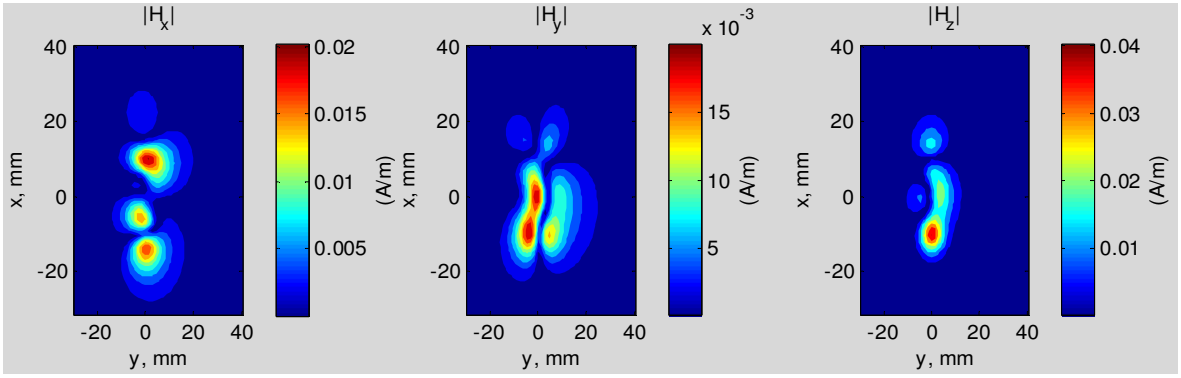

(a)

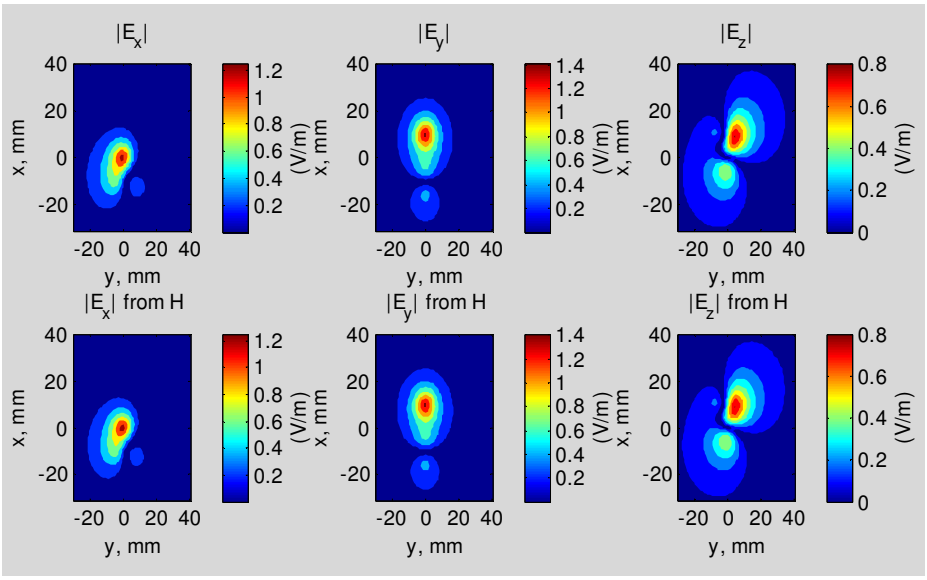

(b)

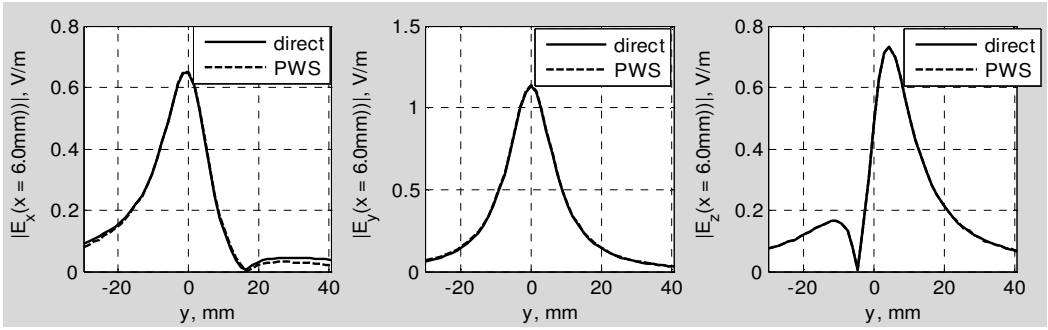

(c)

Fig. 4: Cartographies of the EM radiated by the magnetic dipoles shown in Fig. 3.a at the height, z = 8 mm: considered H-field components (a) and comparisons between the direct calculation and extracted E-field from the H-components maps (b) and profiles (c).

It is worth noting that when the evanescent wave contributions are neglected (operation realized by taking $k_z = 0$ if $k_x^2 + k_y^2 > k^2$), one gets the mapping results displayed in Fig. 5. One can see that the extracted electric field components E_x and E_y and of course the total module $|E|$ are completely different to the reference results from the direct calculations. It means that the computation results are absolutely incorrect and the introduced method is falsified. As forecasted in theory, this finding evidences and illustrates undeniably the importance of the evanescent wave consideration in near-filed.

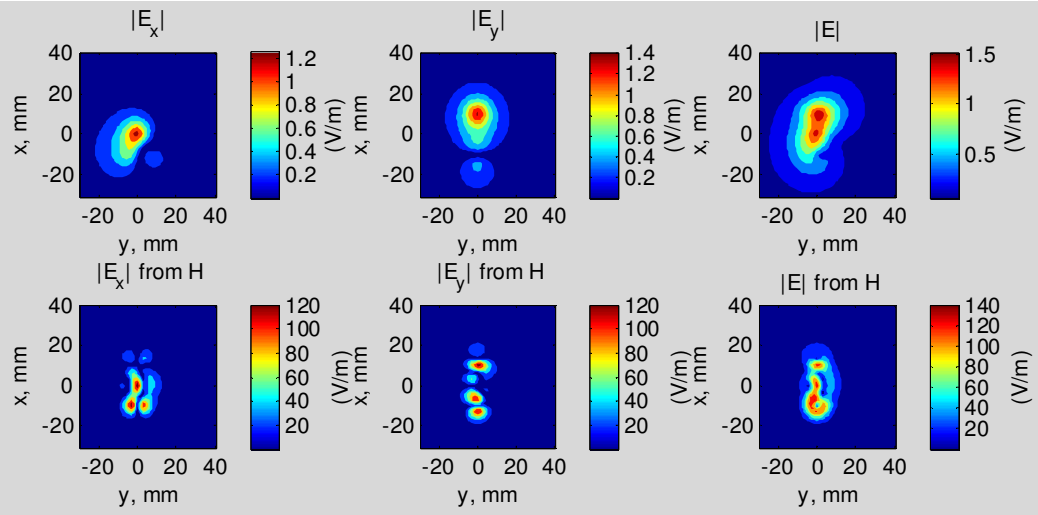

Fig. 5: Comparisons of $|E_x|$ and $|E_y|$ component modules directly calculated and those extracted from the H-field by neglecting the evanescent wave contributions at $z = 8$ mm.

One assumes as given data the H-field maps indicated in Fig. 6.a. As evidenced by the cartographies of Fig. 6.b and the profiles plotted in Fig. 6.c, one gets, once again, a good agreement between the reference analytical E-field components and the calculated ones from the H-field. The slight differences between the plotted direct calculated analytical- and extracted- E-field profiles can be highlighted by the numerical calculation errors. To cope with this computation default, more accurate mesh sizes should be considered.

As conclusion, all these Matlab results allow to confirm the relevance of the proposed E-field extraction technique. As developed in [8], any EM field radiation scanned in 2D map can be equivalent to the radiation of the association of either electric or magnetic dipoles. To get more insight about the feasibility of this concept, further investigation was also made in the next section with the measured EM field radiated by an open-end microstrip TL.

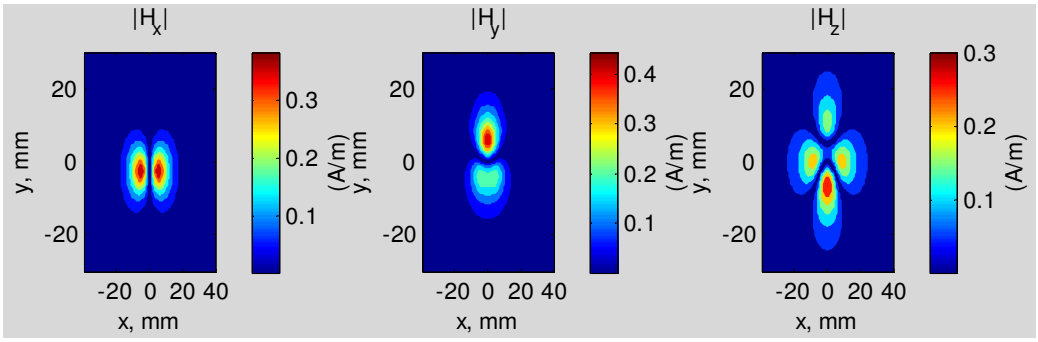

(a)

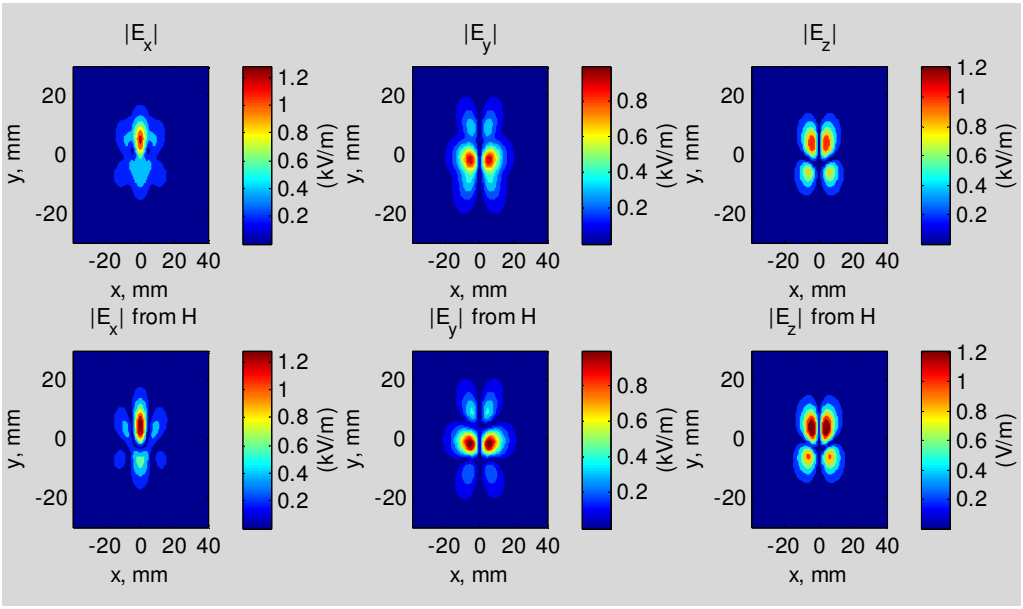

(b)

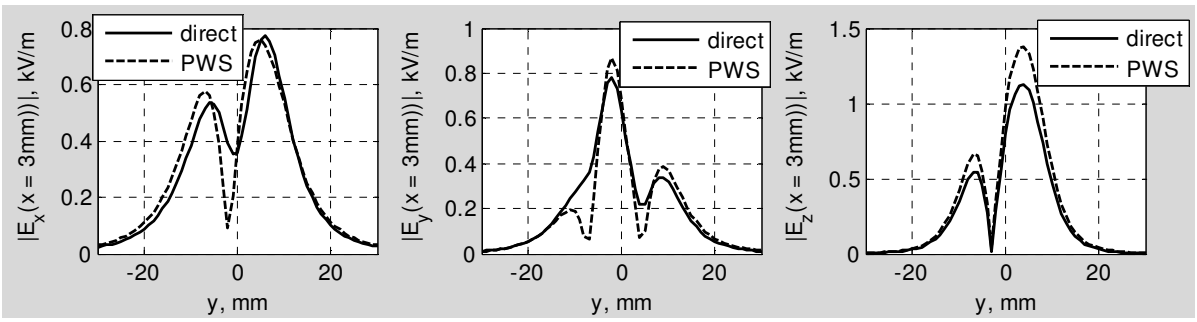

(c)

Fig. 6: Cartographies of EM-fields radiated by the electric dipoles shown in Fig. 1(b) for z = 8 mm: considered H-field components (a) and comparisons between the direct calculation and extracted E-field from the H-components maps (b) and profiles (c).

4. SIMULATION AND EXPERIMENTAL VALIDATIONS

Figs. 7 below present the tested and the 3D design with the EM simulator HFSS™ from Ansoft of the manufactured open-end TL with length, L = 41.2 mm, width, w = 3 mm and thickness, T = 0.035 mm. It was implemented in planar microstrip technology and printed on the epoxy FR4-substrate with permittivity, ε_r = 4.4 and thickness, h = 1.6 mm. With HFSS, this structure was simulated by considering a 3D rectangular box with dimensions, L_x x L_y x L_z = 210 mm x 170 mm x 100 mm and excited by 1W-waveport source at the operating frequency, f = 1 GHz.

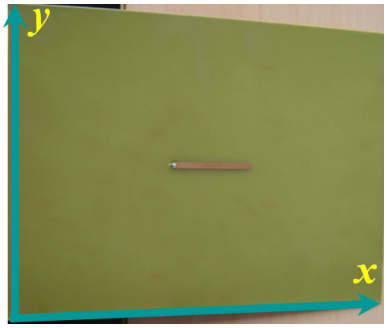

Fig. 7.a: Photograph of the tested device (L_x x L_y = 210 mm x 170 mm).

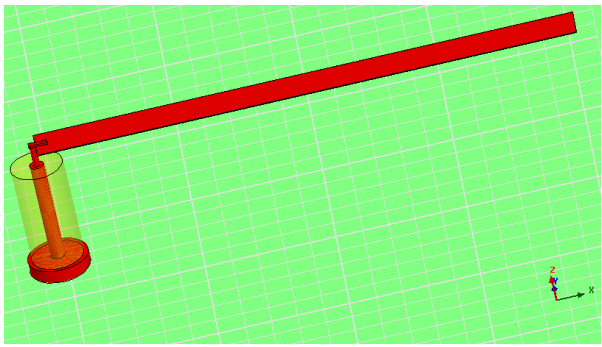

Fig. 7.b: HFSS^{TM} design of the under study TL (L x w x T = 41.2 mm x 3 mm x 0.035 mm) fed by 1-W-waveport source through a coaxial connector.

Therefore, after the near-field scan in the horizontal plane (x = 110 mm and y = 60 mm) placed at the height, z = 5 mm above the metallic line [21], one gets the cartographies of the horizontal H-field components shown in Fig. 8 below. The resolution of this field map was $\Delta x = \Delta y$ = 2 mm. At this stage, we underline that as reported in [15, 16, 17, 21], the vertical component, $H_z(x,y)$ can be merely calculated from $H_x(x,y)$ and $H_y(x,y)$. For doing so, we have calculated $H_x(x,y)$ and $H_y(x,y)$ PWS with expression (5-b) and then, deduce $H_z(x,y)$ from (12).

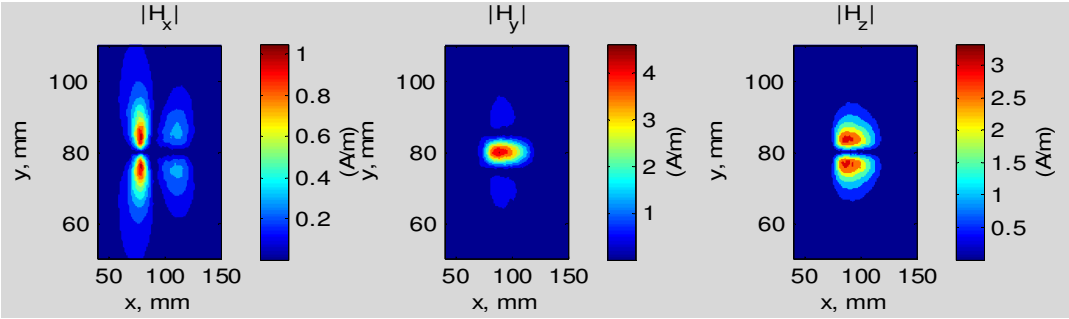

Fig. 8: Magnitude of the measured magnetic field components, $|H_x|$, $|H_y|$ and $|H_z|$ scanned at z = 5 mm above the metallic line.

Therefore, as forecasted in theory, the calculated H_z-field map is very well-correlated to the measured one as displayed in Fig. 9. Moreover, the profiles of these field components in the vertical cut plane placed at the position, x = 100 mm plotted in the right of this figure are also in very good agreement with relative error accurately lower than 2-%. In addition, the profiles of these field components in the vertical cut plane placed at

the position, x = 100 mm plotted in the right of this figure are also in very good agreement with relative error accurately lower than 2-%.

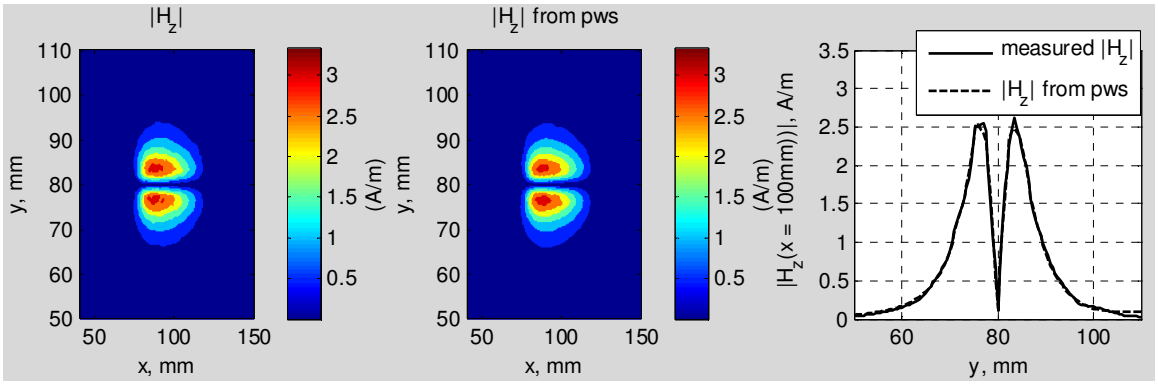

Fig. 9: Comparison between the measured $|H_z|$-component and that one calculated with PWS method.

From these three H-field components, one deduces the E-field ones by proceeding with the work flow indicated in Fig. 2. As results, one obtains the mapping field shown in Fig. 10 below. As illustrated in this figure, one can see that the calculated E-field component maps agree with the HFSS-simulations despite of the slight differences caused by the numerical computation inaccuracy.

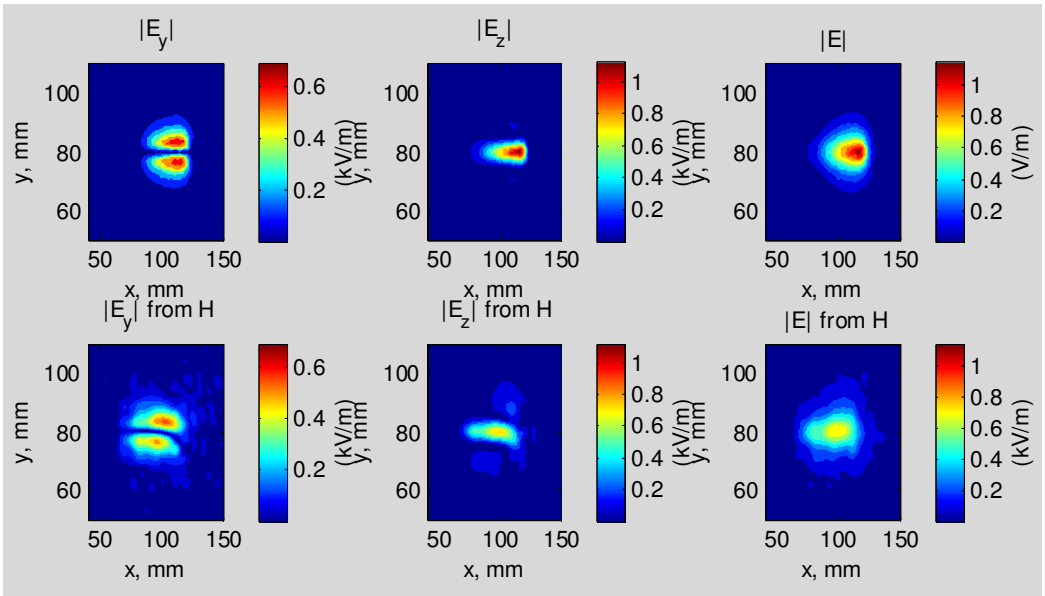

Fig. 10: Comparison of the E-field component maps simulated with HFSS (in top) and the calculations with PWS technique from the H-field shown in Fig. 8 (in bottom).

Furthermore, to get more convincing insight of these results, comparisons between the calculated and the simulated results profiles of $|E_y|$, $|E_z|$ and $|E|$ cut in the vertical plane placed at x = 100 mm have been also made and the results are presented in Fig. 11. Once again, a good agreement between the simulation and the calculation is observed. For this study, it is interesting to note that acting as a quasi-TEM mode, the E_x component radiated by the tested structure is almost negligible compared to E_y and E_z.

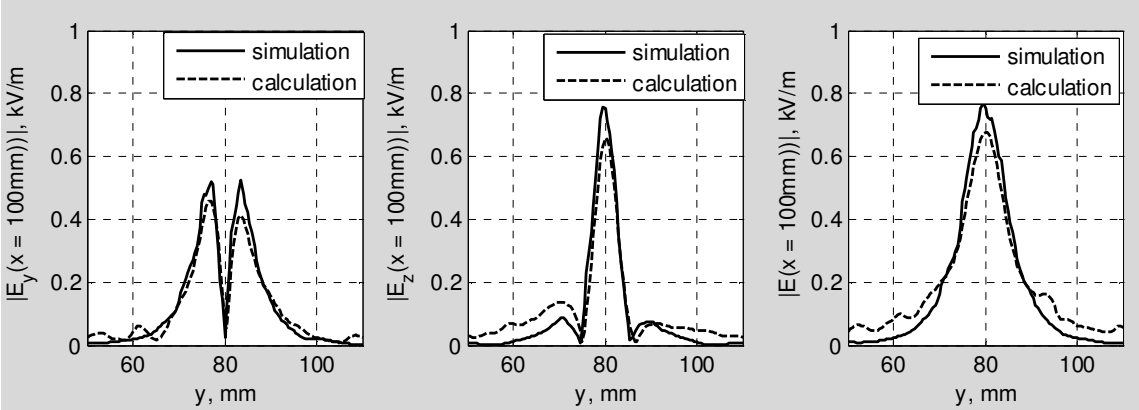

Fig. 11: Comparison of the simulated (full line) and calculated (dashed line) E-field profile in the vertical plane placed at x = 100 mm.

As remark, we point out that to achieve this quality of numerical results, we have oversampled the measured H-field data by considering the lower resolution, $\Delta x = \Delta y = 0.5$ mm. However, this higher resolution enables us to attain better precision. Obviously, it requires large computer resources with regard to main memory and computing time for the lower resolution.

5. CONCLUSION

A computational procedure for extracting the E-field components, E_x, E_y and E_z, knowing only the 2D H-field components, H_x and H_y, is presented and validated successfully both analytically and experimentally, in near field domain. The originality of this work lies on the consideration of the evanescent waves. The concept of the proposed technique is fundamentally based on the use of the Maxwell-Ampere relation combined with the PWS method. In our knowledge, till now, few results were published about the application of this PWS method with the real electronic devices in near field approach (distance, z between the mapping plan of EM-field is lower than the tenth of the wavelength, λ or $z << \lambda/10$) [15-24].

After a detailed description of the proposed methodology, we proceeded with the practical validations with two examples of radiating structures. The first one consists in the analysis of the elementary magnetic and electrical dipole radiations flowed by the harmonic current having operating frequency equal to 1 GHz. Then, the feasibility of the under study technique was also verified with a planar microstrip open-end TL operating also at the same frequency. After the implementation of the analytical expressions into Matlab program, we determined the expected E-field components E_x, E_y and E_z from the 2D H-field components, H_x and H_y. Therefore, as expected in theory, a good agreement between the direct calculated or simulated E-field components and those extracted from the proposed PWS method was found in near field domain. We underline also that a numerical and experimental confirmations of a classical computation technique see relation (12) enabling to deduce the third vertical components, H_z from the two others horizontal components, H_x and H_y was evidenced. We point out that the method presented here, is very important and useful, in particular, for the EMC studies, because it enables the mapping computations of the six E- and H-field components with very less number of measurements. In the continuation of this work, the application of the proposed technique for the EMC test of radiating active devices with multi-tone emission and in time domain is in progress. Then, in the scope of the microwave device

immunity analysis, further investigation is also performed for the modeling of the coupling between non-plane waves and microstrip lines at RF frequencies. Finally, by analogy, we think that the presented technique can be extended also for the case of the other natures of the propagating wave in physical domains such as acoustic-[26], thermal-, quantum- and even seismic-waves, etc …

ACKNOWLEDGEMENT

Acknowledgement is made to Aerospace Valley cluster for the support of this research through EPEA program.

REFERENCES

[1] F. Klotz, in *Proc. of 18th Int. Symp. EMC*, *Zurich*, *2007*, pp. 73-78.

[2] B. D. Sonia, M. Ramdani and E. Sicard, in *Electromagnetic compatibility of integrated circuits. Techniques for low emission and susceptibility*, (Springer, New York, Eds. 2006) p. 464.

[3] R.Perdriau, M. Ramdani, J.L. Levant and A.M. Trullemans, in *Proc. of IEEE Int. Symp. on Industrial Electronics*, *Ajaccio (France)*, *2004*, **14-7**, pp. 193-198.

[4] J.E. Bringas, in *Handbook of Comparative World Steel Standards*, 3rd edn., (ASTM International, 2004), p. 18.

[5] http://www.iec.ch/zone/emc/emc_cis.htm

[6] http://telecom-info.telcordia.com/site-cgi/ido

[7] B. Essakhi, D. Baudry, O. Maurice, A. Louis, L. Pichon and B. Mazari, *Eur. Phys. J. Appl. Phys.* **38**, 275 (2007).

[8] M. Iwanami, E. Yamazaki, K. Nakano, T. Sudo, S. Hoshino, S. Wakana, M. Kishi and M. Tsuchiya, *J. Lightwave Technology*, **21**(12), 3273 (2003).

[9] Y. Vives-Gilabert, C. Arcambal, A. Louis, F. Daran, P. Eudeline and B. Mazari, *IEEE Tran. EMC* **49**(2), 391 (2007).

[10] R. Rammal, M. Lalande, E. Martinod, N. Feix, M. Jouvet, J. Andrieu and B. Jecko, *Int. J. Ant. Prop.*, *Hindawi*, 2009.

[11] P. Malcovati and F. Maloberti, *Aerospace and Electronic Systems Magazine*, **14**(9), 43, 1999.

[12] J.M. Bakhashwain, M.H. Shwehdi, U.M. Johar and A.A. Al-Naim, in *Proc of ICNIR*, (Uniten, 2003).

[13] T. Tajima, A. Burrell, G. Eremeev, V. Dolgashev, D. Martin, C. Nantista, S. Tantawi, C. Yoneda, B.H. Moeckly and I. Campisi, *IEEE ECNF*, **11**, 2010.

[14] F. Hongmei, in *Proc. of IEEE EMC Symp.*, *Austin*, *2009*, pp. 321-324.

[15] C.A. Balanis, in *Antenna theory: Analysis and design*, 3rd edn., (Wiley, New York, 2005).

[16] D.T. Paris, W.M. Leach and E.B. Joy, *IEEE Tran. Ant. Prop.*, **26**(3), 373, 1978.

[17] J.J.H. Wang, *IEEE Tran. Ant. Prop.*, **36**(6), 741, 1988.

[18] G.F. Masters, in *Proc. of AMTA Conf.*, 1991.

[19] J. Shi, M.A. Cracraft, K.P. Slattery M. Yamaguchi and R.E. DuBroff, *IEEE Tran. EMC* **47**(3), 642 2005.

[20] M. Cauterman, I. Seignolles, D. Lecointe and J.C. Bolomey, In *Proc. of Workshop on EMC Measurement Techniques for Complex and Distributed System*, *Lille*, *France*, 2001.

[21] P.S.H. Leather and J.D. Parsons, *Electron. Let.*, **39**(25), 2003.

[22] J. Shi, M.A. Cracraft, J. Zhang and R.E. DuBroff, in *Proc. of IEEE Ant. Prop. Int. Symp.*, San Jose, CA (USA), **3**, 1477, 1989.

[23] H. Junji and T. Yoshiaki, in *Proc. of 18th Int. Zurich Symposium on EMC*, Munich 2007.

[24] D. Baudry, M. Kadi, C. Arcambal, Z. Riah, Y. Vives, A. Louis and B. Mazari, *Science, Measurement & Technology*, *IET*, **3**(1), 72 2009.

[25] B. Ravelo, *PIER B Journal*, **25**, 171, 2010.

[26] M.Y. Gureev and M.A. Mironov, *Akustičeskij žurnal*, **53**(6), 774, 2007.